ICES Journal of Marine Science

ICES Journal of Marine Science (2015), 72(6), 1942–1951. doi:10.1093/icesjms/fsv046

Contribution to the Themed Section: '*Revisiting Sverdrup's Critical Depth Hypothesis*'

Original Article

Physiological constrains on Sverdrup's Critical-Depth-Hypothesis: the influences of dark respiration and sinking

Christian Lindemann[1]*, Jan O. Backhaus[2], and Michael A. St John[1]

[1]*National Institute of Aquatic Resources – DTU Aqua, Technical University of Denmark, Jægersborg Allé 1, Charlottenlund 2920, Denmark*
[2]*Institute of Oceanography, University of Hamburg, Bundesstraße 53, Hamburg 20146, Germany*

**Corresponding author: tel: +45 35 88 34 47; fax: +45 35 88 33 33; e-mail: chrli@aqua.dtu.dk*

Lindemann, C., Backhaus, J. O., and St John, M. A. Physiological constrains on Sverdrup's Critical-Depth-Hypothesis: the influences of dark respiration and sinking. – ICES Journal of Marine Science, 72: 1942 – 1951.

Received 11 June 2014; revised 25 February 2015; accepted 1 March 2015; advance access publication 24 March 2015

Discussions on the controls initiating the onset of the phytoplankton spring bloom in particular in the North Atlantic have since Sverdrup been dominated by the role of physical and biological drivers. Undoubtedly, these drivers play an important role in phytoplankton dynamics and thus the onset of the spring bloom. However, they neglect the cells ability to modify vital rates in response to changes in the external environment. In this study, we use a non-hydrostatic convection model coupled to an Individual-Based-Model to simulate changes phytoplankton cells during the transition from winter conditions as driven by convective mixing, and the onset of thermal stratification resulting in the spring bloom. The comparison between a simulation using a standard fixed rate approach in line with the original Sverdrup hypothesis and a simulation parameterized to include variable respiration and sinking rates showed that the latter approach was able to capture the observed phytoplankton concentration during deep convective mixing, the timing and magnitude of the spring bloom as well as simulating realistic physiological rates. In contrast, the model employing fixed rate parameterizations could only replicate field observations when employing unrealistic parameter values. These results highlight the necessity to consider not only the physical and biological external controls determining phytoplankton dynamics but also the cells ability to modify critical physiological rates in response to external constraints. Understanding these adaptive qualities will be of increasing importance in the future as species assemblages and physical controls change with changing climate.

Keywords: cell sinking, dark respiration, deep convection, phytoplankton spring bloom.

Introduction

The onset of the North Atlantic phytoplankton spring bloom has received a significant amount of attention due in part its influence on the dynamics of higher trophic levels (Houde, 2008) and its role for the biological carbon pump (Sanders *et al.*, 2014). The "Critical-Depth-Hypothesis" (Sverdrup, 1953) with its foundations in the works of Gran and Braarud (1935) and Riley (1946) has served as the starting point for predicting the onset of the spring bloom. It has been widely discussed, criticized, and extended based on increased understanding of the role of abiotic and biotic mechanisms. For example, Eilertsen *et al.* (1995) based on the role of light on phytoplankton proposed photoperiod control as a driving mechanism for the onset of the spring bloom. Moreover, the "Critical-Turbulence-Hypothesis" (Huisman *et al.*, 1999) predicts bloom conditions based on turbulent diffusivity, light-limited growth, and mixed-layer depth. Following this mechanism, low levels of turbulent diffusivity are not able to counteract cell sinking, while high levels of turbulence mix cells out of the euphotic zone. At an intermediate level, sinking is balanced by turbulent mixing, retaining the cells in the euphotic zone where they receive sufficient light to generate a surface phytoplankton bloom. The "Convection-Shutdown-Hypothesis" (Ferrari *et al.*, 2014) builds upon earlier findings by Townsend *et al.* (1994) and Taylor and Ferrari (2011a) and suggested that the shutdown of winter convective mixing could serve as a better indicator for the onset of the spring bloom than the mixed-layer depth, the basis of the "Critical-Depth-Hypothesis". This approach has subsequently been interpreted as an extension of Huisman's "Critical-Turbulence-Hypothesis"

(Behrenfeld and Boss, 2014). Furthermore, processes such as frontal systems (Taylor and Ferrari, 2011b) and vertical processes (Mahadevan *et al.*, 2012) can play an important role in creating stratification and thus initiating surface blooms without a change in net surface heat flux. All of these mechanisms infer physical controls as the primary cause of the rapid increase in surface chlorophyll observed in early spring. A more biologically based interpretation of the controls on the spring bloom has been presented by Behrenfeld (2010). The "Disturbance-Recovery-Hypothesis" suggesting that phytoplankton blooming is predominately controlled by biological interaction, namely the release of grazing pressure due to dilution of microzooplankton grazers (Landry and Hassett, 1982; Behrenfeld and Boss, 2014).

Given the multiple and interrelated mechanisms acting to influence the phytoplankton community, it is unlikely that one dominant mechanism, biological or physical in nature controls phytoplankton growth and the onset of the spring bloom. More likely, these dynamics are controlled by an interplay between the aforementioned mechanisms with one or the other dominating spatially and or temporally and leading to the heterogeneous manifestation of the bloom as seen in satellite (Lindemann and St John, 2014).

An omission in the discussion to date has been the basic physiological ability of phytoplankton to modify their vital rates relative to their external conditions. The Critical-Depth-Hypothesis (Sverdrup, 1953) assumes a constant respiration rate, encompassing grazing, sinking and cell respiration, independent of depth and the diurnal cycle. This does not reflect the cells ability to modify critical rates such as respiration and sinking, which potentially lead to a change in the critical depth (Smetacek and Passow, 1990).

Cell respiration is a highly variable internal process influenced by environmental conditions such as temperature (Verity, 1982), nutrients (Laws and Bannister, 1980), and light (Falkowski and Owens, 1980) as well as cellular growth. Light-limited low growth rates can induce a reduction of metabolic rates and thus dark respiration (Jochem, 1999). Based on laboratory studies, Falkowski and Owens (1980) determined that for cells acclimatized to a specific light level, the ratio of maximum production and dark respiration remained the same over a wide variety of light intensities suggesting that the maximum growth and respiration rates can be equally affected by light. This observation was supported in subsequent studies, e.g. Cosper (1982), Verity (1982), Langdon (1988), and Sakshaug *et al.* (1989).

However, in the North Atlantic during winter, within the deep convective layer, cells can be exposed to rapidly changing light levels, thus not conforming to the assumption of constant light or a steady state. Investigations on short-term dark respiration responses to changing light conditions have shown that dark respiration increases rapidly with photosynthesis (Weger *et al.*, 1989). As light declines, photosynthesis declines commensurate with the reduction in light; however, dark respiration does not react instantaneously but decreased gradually to a minimum (Weger *et al.*, 1989; Xue *et al.*, 1996). This decoupling of photosynthesis and respiration results in proportionally higher rates of respiration after light exposure (Falkowski *et al.*, 1985).

Phytoplankton cells have been observed to exhibit a wide range of different sinking rates, from several meters per day (Smayda, 1970) to positive buoyancy (Acuña *et al.*, 2010). For cells of similar shape and density, the sinking speed can be estimated using Stokes law (Miklasz and Denny, 2010). However, density is influenced by the species-specific cell composition and growth phase. Cells can maintain density levels close to neutral buoyancy, or even achieve positive buoyancy (Acuña *et al.*, 2010) via active regulation of inorganic (Anderson and Sweeney, 1977) and organic material (Boyd and Gradmann, 2002). Buoyancy regulation and hence the sinking rate of phytoplankton cells has been related to growth (Waite *et al.*, 1992; Brookes and Ganf, 2001). Fast growing cells typically are found to show lower sinking rates than cells growing under conditions of limiting light (Waite *et al.*, 1992), nutrients (Bienfang *et al.*, 1982) or iron (Waite and Nodder, 2001), independent of cell size. These observations suggest that growth conditions are more important in controlling cell sinking than cell size (Bienfang *et al.*, 1982; Peperzak and Colijn, 2003).

To assess the importance of the cells ability to modify dark respiration and sinking, we developed and employed an Individual-Based-Model (IBM) for phytoplankton cells. IBM models have proven to be a useful tool for understanding the growth dynamics of phytoplankton cells (Hellweger and Kianirad, 2007). One of the advantages of the Lagrangian approach relative to the Eulerian approach is that an individual particle can be followed through space and time. Thus, the individual history of one particle cannot only be stored for analysis, but particle properties can depend on the "life history" as well as the abiotic and biotic constraints impacting on the individual. In this study, using a non-hydrostatic convection model (CM) coupled to a Lagrangian IBM, we investigate the effect of the cells natural ability to adjust their respiration and sinking in relation to changes in environmental conditions over the course of the onset of the spring bloom.

Material and methods

Non-hydrostatic convection model

The non-hydrostatic CM utilized has been employed in several studies (Kämpf and Backhaus, 1998; Backhaus *et al.*, 1999; Wehde and Backhaus, 2000; Wehde *et al.*, 2001; Große *et al.*, 2014) and is set on an isotropic, equidistant grid. The model uses Boussinesq-equations for an incompressible fluid to describe a 2.5 dimensional ocean slice. The ocean slice itself is two dimensional (x,z); however, fluxes are calculated for all three dimensions (x,y,z). The equations for conservation of movement are as follows:

$$\frac{\partial U}{\partial t}+U\frac{\partial U}{\partial x}+W\frac{\partial U}{\partial z}-fV+f^{\circ}W=-\frac{1}{\rho_0}\frac{\partial P}{\partial x}+\frac{\partial}{\partial x}\left(\nu_t\frac{\partial U}{\partial x}\right)+\frac{\partial}{\partial z}\left(\nu_t\frac{\partial U}{\partial z}\right), \quad (1)$$

$$\frac{\partial V}{\partial t}+U\frac{\partial V}{\partial x}+W\frac{\partial V}{\partial z}+fU=\frac{\partial}{\partial x}\left(\nu_t\frac{\partial V}{\partial x}\right)+\frac{\partial}{\partial z}\left(\nu_t\frac{\partial V}{\partial z}\right), \quad (2)$$

$$\frac{\partial W}{\partial t}+U\frac{\partial W}{\partial x}+W\frac{\partial W}{\partial z}-f^{\circ}U=-\frac{1}{\rho_0}\frac{\partial P}{\partial x}-\frac{\rho'}{\rho_0}g+\frac{\partial}{\partial x}\left(\nu_t\frac{\partial W}{\partial x}\right)+\frac{\partial}{\partial z}\left(\nu_t\frac{\partial W}{\partial z}\right), \quad (3)$$

where U, V, and W are the velocity components for the three dimensions (x,y,z). The variable P denotes the non-hydrostatic part of the pressure, g represents the gravity, ν_t the eddy viscosity, ρ' the reduced density, and ρ_0 represents the reference density. The variables f and f° are the complete Coriolis parameters. The turbulent eddy viscosity (ν_t) is parameterized by the zero-order turbulence closure by Kochergin (1987). The numerical stability is ensured by the CFL stability criteria with a physical time steps for advection of temperature, salinity, and momentum set to a maximum of 1 min.

The equations of conservation for temperature (T) and salinity (S) are:

$$\frac{\partial T}{\partial t} + U\frac{\partial T}{\partial x} + W\frac{\partial T}{\partial z} = \frac{\partial}{\partial x}\left(K_T\frac{\partial T}{\partial x}\right) + \frac{\partial}{\partial z}\left(K_T\frac{\partial T}{\partial z}\right) + \frac{\delta E_T}{\partial t}, \quad (4)$$

$$\frac{\partial S}{\partial t} + U\frac{\partial S}{\partial x} + W\frac{\partial S}{\partial z} = \frac{\partial}{\partial x}\left(K_S\frac{\partial S}{\partial x}\right) + \frac{\partial}{\partial z}\left(K_S\frac{\partial S}{\partial z}\right) + \frac{\delta E_S}{\partial t}, \quad (5)$$

where $\delta E_T/\partial t$ and $\delta E_s/\partial t$ are the thermal and saline sea surface forcing, respectively. The variables K_T and K_S are the eddy diffusivities for heat and salt, respectively, and are set equal to the eddy viscosity (ν_t).

The thermal surface forcing changes according to

$$\frac{\delta E_T}{\partial t} = \frac{-Q_{net}}{\rho c_{sw}}, \quad (6)$$

where c_{sw} is the specific heat of seawater. The variable Q_{net} denotes the net surface heat flux calculated by

$$Q_{net} = \Delta Q_{lw} + Q_{sw} + Q_{lat} + Q_{nses}, \quad (7)$$

where $\triangle Q_{lw}$ is the difference between the atmospheric long-wave radiation and the long-wave radiation from the sea surface, Q_{sw} is the incoming short wave radiation, Q_{lat} is the latent heat flux, and Q_{sens} is the sensible heat flux.

Light intensity (I) in the water column at depth (z) is described by

$$I(z) = I_0 \times \exp^{-(k_e+s)z}, \quad (8)$$

where I_0 is the incoming radiation at the sea surface, z is the depth, k_e is the extinction coefficient due to turbidity, and s the self-shading of phytoplankton estimated by

$$s = k_{phy}C, \quad (9)$$

where k_{phy}, the extinction coefficient of phytoplankton, is 0.03 (Große *et al.*, 2014) and C is the phytoplankton concentration in (mmol C m^{-3}).

For further details of the physical model, see Kämpf and Backhaus (1998) and Wehde and Backhaus (2000). Deviating from the older versions of this model, this version uses the equation of state proposed by McDougall *et al.* (2003), which uses potential temperature instead of the *in situ* temperature (UNESCO, 1981).

Biological Individual-Based-Model

The biological IBM consists of Lagrangian tracers depicting phytoplankton cells of indefinite biomass within the ocean slice where the biological time step is set to 5 min.

Phytoplankton growth during winter and early spring in the North Atlantic is not believed to be nutrient limited, therefore it does not account for nutrient limitation. Grazing is not accounted for explicitly, but it is parameterized by a biomass-dependent mortality rate (m). All biological parameter values are given in Table 1.

Cell growth

Net phytoplankton concentration depends on the cells growth rate μ, the cells sinking rate v, and advection and diffusion in the three dimensions:

$$\frac{DC}{Dt} = \frac{\partial C}{\partial t} - \nabla\cdot(UC) + \nabla\cdot(\nu_t\nabla C) - v\frac{\partial C}{\partial z} + \mu C, \quad (10)$$

where U = (U,V,W). The growth rate is estimated by

$$\mu = P^C - r - m, \quad (11)$$

where P^C is the photosynthesis, r is the respiration, and m is the mortality.

Photosynthesis is calculated according to:

$$P^C = P^C_{max}\left[1 - \exp\left(-\frac{\alpha^{chl}I\theta^C}{P^C_{max}}\right)\right], \quad (12)$$

where P^C_{max} is the maximum specific photosynthesis rate, α^{chl} is the initial slope of the function, and θ^C is the chlorophyll-to-carbon ratio. Changes in chlorophyll are described following Geider et al. (1997):

$$\frac{\mathrm{dChl}}{\mathrm{d}t} = \rho^{chl}P^C C - r\mathrm{Chl}, \quad (13)$$

where ρ^{chl} is the biosynthesis of chlorophyll according to

$$\rho^{chl} = \theta^C_m\left(\frac{P^C}{\alpha^{chl}I\theta^C}\right), \quad (14)$$

where θ^C_m is the maximum chlorophyll-to-carbon ratio.

Table 1. Biological model parameters and scaling coefficients.

Description	Symbol	Value	Unit	Source
Maximum specific carbon fixation rate	P^c_{max}	3	d^{-1}	Geider *et al.* (1998)
Chl-specific initial slope of PI curve	α^{chl}	0.5	10^{-5} gC m^{-2} (gChl mmol photons)$^{-1}$	Geider *et al.* (1997)
Maximum Chl-to-carbon ratio	θ^{chl}_m	0.05	gChl (gC)$^{-1}$	Cloern *et al.* (1995)
Cost of biosynthesis	Z	0.23	gC (gC)$^{-1}$	Geider *et al.* (1998)
Mortality rate	m	0.05	d^{-1}	Wehde *et al.* (2001)
Specific respiration reduction in dark	α^r	0.0455	h^{-1}	Weger *et al.* (1989)
Maintenance cost	r^0	0.02	gC (gC)$^{-1}$	Geider and Osborne (1989)
Maximum sinking velocity	v^{max}	6.8	m d^{-1}	Smayda (1970)[a]
Sinking rate scaling coefficient	α^v	4.15	–	Waite *et al.* (1992)

[a]Only considering alive cells.
The values for the specific respiration reduction in the dark and the sinking rate scaling coefficient were extracted from Weger *et al.* (1989) and Waite *et al.* (1992), respectively.

Cell respiration

In this model, cell respiration rate consists of maintenance metabolism (r^0) and the cost of biosynthesis which, under the influence of light, is proportionally related to photosynthesis. However, when photosynthesis ceases, biosynthesis does not stop immediately, but decays over time (e.g. Walter *et al.*, 2015). Weger *et al.* (1989) investigated short-term acclimation of phytoplankton dark respiration to variable light conditions. While the shutdown of light led to a gradual decrease of respiratory loss, moving from dark to light conditions showed an almost instantaneous return of high respiration rates. Here, the respiration rate is modelled accounting for these dynamics through:

$$r = \max\begin{pmatrix} \varsigma P^C + r^0 \\ r \times \exp^{\alpha^r} \end{pmatrix}, \tag{15}$$

where the upper term represents respiration in light with ζ being the cost of biosynthesis. The second expresses the decrease of respiration in the dark, where α^r is the rate of decrease with time, which was extracted from Weger *et al.* (1989).

Cell sinking

The sinking rate of each cell is modelled based on the concept of Waite *et al.* (1992), who coupled the sinking rate to the overall metabolic state of the cell. They found that when cells were transferred from light into darkness, their sinking rate could be described as a negative function of their respiration rate.

The sinking rate can therefore be described by the maximum sinking velocity $v_{\max}$ and a scaling factor (α^v) of the relative respiration (r'), which was extracted from Waite *et al.* (1992):

$$v = {v_{\max}}^{-\alpha^v r'}, \tag{16}$$

where

$$r' = \frac{r}{\zeta P^C_{\max} + r^0}. \tag{17}$$

Model setup and initial conditions

The model was set up to simulate conditions at Ocean Weather Station Mike (OWM) (66°N 02°E), the same station where the observations by Sverdrup (1953) were used to develop the Critical-Depth-Hypothesis. Three hourly meteorological forcing for the period was obtained from the Norwegian Meteorological Office (METNO) and was used for the simulation from 5 April to 10 May 1997 (yearday 95–130) with the first 5 d considered as spin-up. The simulation was initialized with vertical profiles from Ocean Weathership Mike. This period was chosen since it encompassed the period from pre-bloom conditions with typical deep convective mixing to stratified conditions with shallow wind-driven mixing towards the end of the simulation. Here (and in the following) we refer to deep convection as convection that is not driven by nocturnal cooling, but extends over a longer period, hence leading to deeper convective mixing. The simulation was not continued throughout the full spring bloom as our assumptions (e.g. no nutrient limitation) would be invalid. Field observations of the further development of the spring bloom after our simulation period showed the maximum chlorophyll concentration occurred on 23 May (yearday 143) with values of over 3 mg Chl m^{-3} (Niehoff *et al.*, 1999).

In our study, Lagrangian tracers (20 000 particles) were randomly distributed from 10 to 400 m depth at the beginning of the simulation. The model domain was set to 1000 × 1500 m with a grid size of 5 × 5 m.

Model simulations

To demonstrate the effect of the cells ability to modify rates of both sinking and respiration, we compared the model simulation, using the variable parameterizations for respiration and sinking as described above, to simulations using fixed values. Other than employing the variable parameterizations, both the fixed value simulations and the adaptive simulation are identical. The values used in the simulations with fixed parameter values were chosen to encompass the range of values found in the adaptive simulation. These fixed values were 0.02, 0.135, 0.25, and 0.47 for the daily average carbon-specific respiration (d^{-1}) and 0, 2.25, 4.5, and 6.8 sinking ($m\ d^{-1}$), respectively. We compared the adaptive run to runs with each of the 4 × 4 combinations of these fixed respiration and sinking rates. The outputs of these fixed value simulations and the respective fixed parameter combinations are presented in Figure 5.

Results

The beginning of the simulation is characterized by a negative net surface heat flux (Figure 1a), with minimal values of ca. −350 W m^{-2}. This led to strong convective mixing as indicated by the turbulent kinetic energy (TKE) (Figure 1b). The initial

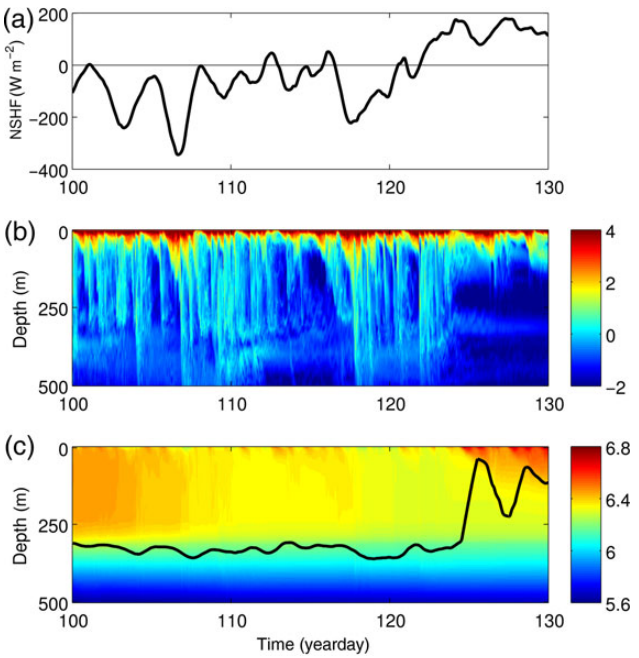

Figure 1. Physical water properties as predicted by the non-hydrostatic CM over the course of the simulation at Ocean Weathership Mike. (a) Simulated net surface heat flux (W m^{-2}). (b) Hovmöller diagram showing simulated water column TKE ($cm^2\ s^{-1}$) on a log scale. (c) Simulated temperature within the water column (°C). The black line indicates the estimated mixed-layer depth.

period of strong mixing was followed by a reduction in net surface heat loss (-100–70 W m^{-2}) causing a reduction in convective mixing, followed by a stabilization of the water column (~5 May, yearday 125) as indicated by the temperature profile (Figure 1c). This resulted in changes in the mixed-layer depth, defined here as the depth range over which the temperature deviates by <0.2°C from 10 m below the surface. This value is on the lower range of values commonly used to define the MLD (de Boyer Montégut *et al.*, 2004). The temperature within the surface layer (~6.3–6.5°C) as predicted by the model compares well with observations and the onset of stratification was captured by the model both with regard to the timing (~5 May, yearday 125) and stratification depth (~50 m) (Irigoien *et al.*, 1998).

Adaptive simulations

The simulated biomass and dynamics of the winter phytoplankton community using the adaptive parameterization compares well with the published 100 m integrated values of Irigoien *et al.* (1998) and Niehoff *et al.* (1999), showing an increase in biomass of ~200% (Figure 2) over the period of the simulation.

Until the onset of stratification, the integrated chlorophyll over the mixed layer showed a decreasing trend (Figure 2). The onset of stratification was marked by a short lived drop in mixed-layer integrated phytoplankton biomass after which the mixed-layer integrated phytoplankton concentration started to increase similar to that of the 100 m integrated chlorophyll. The drop can be attributed to cells being "left behind" below the now stratifying mixed layer, thus reducing the integrated biomass due to a decrease in the water column depth now defining as the mixed layer.

Depending on their position within the water column, the phytoplankton "particles" were either retained within the mixed layer or where "detrained" (Behrenfeld and Boss, 2014) into deeper waters as has been suggested earlier by Evans and Parslow (1985). Our simulations illustrate that during deep convective mixing all tracers are generally homogeneously distributed throughout the mixed layer (Figure 3c). However, occasionally increased production occurred in agreement with the Critical-Turbulence-Hypothesis (Huisman *et al.*, 1999) leading to an increased phytoplankton biomass near the surface. This biomass was however subsequently quickly mixed throughout the convective mixed layer (CML) as result of an increase in turbulent mixing.

A reduction in net surface heat flux after 28 April (yearday 118) (Figure 1a) led to reduced cooling of surface water and thus to a reduction in convection depth. Thereafter, primary production in the upper ~50 m increased with reduced mixing towards the end of the simulation (Figure 3c). The simulated chlorophyll-to-carbon ratio varied between 0.05 and 0.018 with surface values being the lowest, in particular toward the end of the simulation. These values are at the higher end of the range of values reported in the literature (Cloern *et al.*, 1995; Geider *et al.*, 1997), which is however not surprising given the overall low light levels. Dark respiration generally followed the same pattern as primary production. However, because the increase in production did not occur instantaneously, it showed a wider spread over time and space (Figure 3a). Within the euphotic zone, defined as 1% of surface light level, the ratio of integrated daily carbon-specific gross production and integrated daily carbon-specific respiration rate varied in between ~28 and 39% (Figure 4), which compares well with value reported in the literature. Geider (1992) summarized several earlier measurements on phytoplankton respiration finding a range of 26–65% carbon being respired over 24 h. Laws and Bannister (1980) found night losses in between 10 and 20% of daytime production and a more theoretical approach (Marra and Barber, 2004) yielded values of ~35–40% of daily respiratory losses.

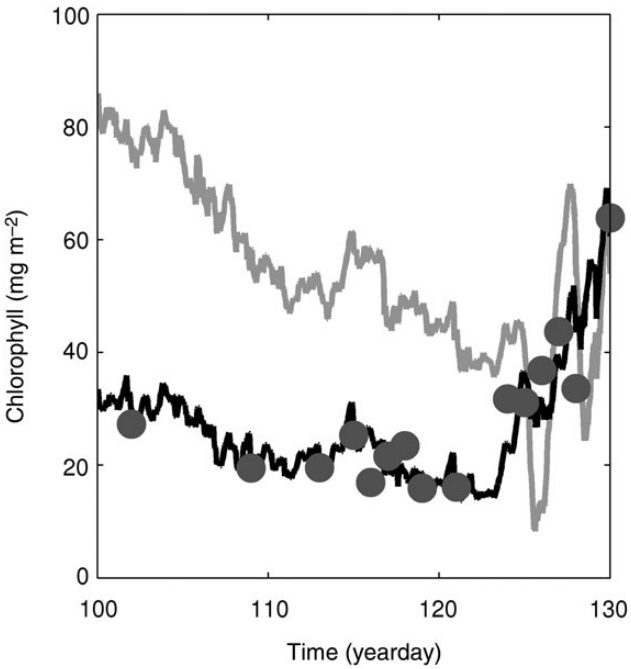

Figure 2. Integrated chlorophyll at Ocean Weathership Mike over the course of the simulation. The solid lines show chlorophyll integrated over the upper 100 m. Grey dots are observations of 100 m integrated chlorophyll. The dashed line shows chlorophyll integrated over the mixed-layer depth and hence over the varying convective layer depth.

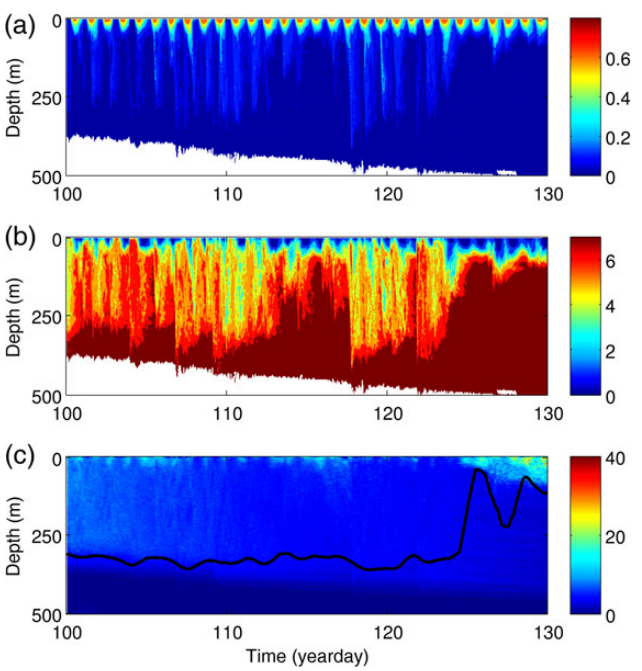

Figure 3. Phytoplankton properties simulated by the non-hydrostatic CM over the course of the simulation at Ocean Weathership Mike. Hovmöller diagrams show the (a) carbon-specific respiration rate (d^{-1}), (b) sinking rate (m d^{-1}), and (c) phytoplankton concentration (mg C m^{-3}).

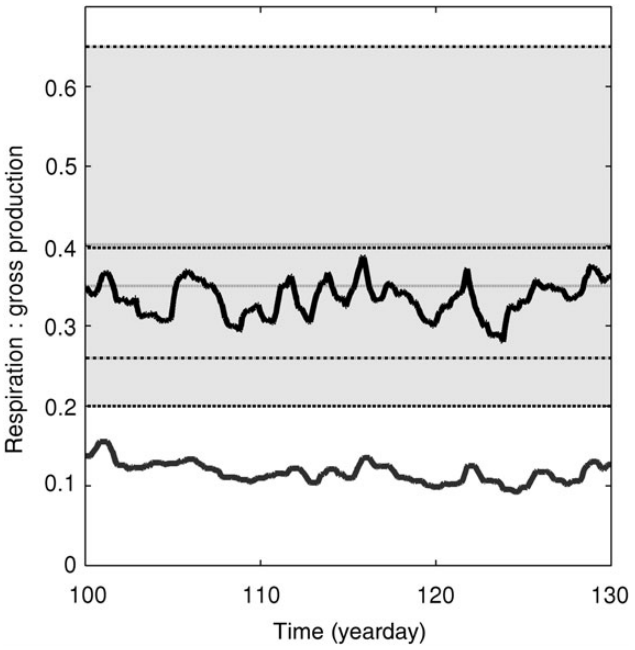

Figure 4. Simulated ratio of daily average respiration rate to daily gross production rate. The thick black line indicates the result as simulated by the adaptive model. The thick gray line indicates the result as simulated using a fixed specific respiration rate of 0.135 d^{-1} and a sinking rate of 4.5 m d^{-1}. The shaded area indicates that the range of values reported in the literature. Vertical lines indicate that limits of range reported by Laws and Bannister (1980) (dash-dotted), Geider (1992) (dashed), and Marra and Barber (2004) (dotted).

Sinking rates were lowest at the surface during this period with rates as low as 0.13 m d^{-1}. Generally, sinking rates increased with depth and were highest below the mixed layer reaching v^{max} of 6.8 m d^{-1} (Figure 3b).

Adaptive vs. fixed parameterizations

We compared the adaptive run to runs with different combinations of fixed respiration and sinking rates (Figure 5). In general, changes in respiration rates had a bigger influence on phytoplankton biomass than sinking rates. Runs with respiration set to the minimum value ($r^0 = 0.02$ d^{-1}) systematically overestimated the phytoplankton biomass regardless of the sinking rate applied. Runs using respiration rates of 0.25 and 0.47 d^{-1} always underestimated phytoplankton concentrations. In the runs using a fixed respiration rate of 0.135 d^{-1}, the simulated phytoplankton concentration showed a much better fit with observations (Figure 5).

The impact of the sinking rate on phytoplankton biomass was more pronounced towards the end of the simulations, despite remaining less important than the respiration rate. In these simulations, using fixed rates, the ratio of daily carbon-specific gross production to respiration within the euphotic zone varied in between 0.09 and 0.15 d^{-1} (Figure 4) which is lower than the lowest values than the values reported in the literature.

Discussion

Phytoplankton biomass

Traditionally, it has been assumed that the peak integrated phytoplankton biomass is associated with the spring bloom. During this period, cells experience sufficient light for growth due to a reduced mixing depth while not under the influence of nutrient limitation, that is, the classical critical-depth model (Sverdrup, 1953). However, the concept of "phyto-convection" (Backhaus *et al.*, 1999) suggests that deep convective mixing can sustain a homogenously distributed viable phytoplankton biomass within the deep winter mixing zone on the same order of magnitude as during the spring bloom (Backhaus *et al.*, 2003). In our simulation, phytoplankton cells are generally homogenously distributed during deep convection which was closely followed by the onset of stratification and an increase in surface phytoplankton biomass (Figure 3c). However, before the onset of stratification around 25 April, a reduction in surface cooling resulted in a net surface heat flux of around zero (Figure 1a). During this period, no change in mixed-layer depth was observed a minor increase in phytoplankton surface concentration occurred (Figure 3c). Similar dynamics have been observed in the North Atlantic (Townsend *et al.*, 1992) and support the hypothesis that the shutdown of deep convective mixing is a better indicator for growth conditions than the hydrostatic vertical water column profile (Townsend *et al.*, 1994; Taylor and Ferrari, 2011a). This pulse of productivity also indicates that the cells contained in an actively mixed layer represent the potentially photosynthetic active phytoplankton. Phytoplankton biomass within the deep CML was observed by Backhaus *et al.* (2003) to be similar to estimates of biomass occurring during the spring bloom. Our model shows similar dynamics with the total standing stock over the CML being on the same order as that after the onset of stratification (Figure 2). Hence, the upper 100 m, a traditional approach for estimating integrated biomass, has the potential to underestimate the standing stock during winter.

Given these observations, the question then arises as to the mechanisms allowing phytoplankton cells to survive and maintain a viable phytoplankton stock in a deep mixed layer where they spend a large period below the euphotic zone. Over the course of winter, the release from micro-zooplankton grazing pressure has been suggested to compensate for the reduction in light exposure as the mixed layer deepens (Behrenfeld and Boss, 2014). Our model does not include an explicit representation of zooplankton grazing pressure; hence, we were not able to address this question. However, the adaptive simulation showed a good fit with field observations without a detailed representation of grazing, suggesting that physiological acclimation could play an equally important role.

Individual physiology of phytoplankton growth

The ability of a phytoplankton cell to react to changing environmental conditions, although a key determinant of biomass production and community structure has received little attention in relation to the onset of the spring bloom.

For an individual cell, the internal growth is dependent upon nutrients, the photosynthetically active radiation for growth and the loss terms such as sinking and respiration, which become proportionally more important under conditions of low growth (Sakshaug *et al.*, 1991).

Sinking

Phytoplankton sinking rates are highly variable and depend on species, cell shape, life stage, growth condition, and particle aggregation (Smayda, 1970; Miklasz and Denny, 2010). Sinking velocities of phytoplankton cells rarely exceed a few tens of meters per day, while actively growing cells have been shown to have much lower sinking velocities and can even achieve positive buoyancy (Moore and Villareal, 1996; Acuña *et al.*, 2010). In a convective regime vertical,

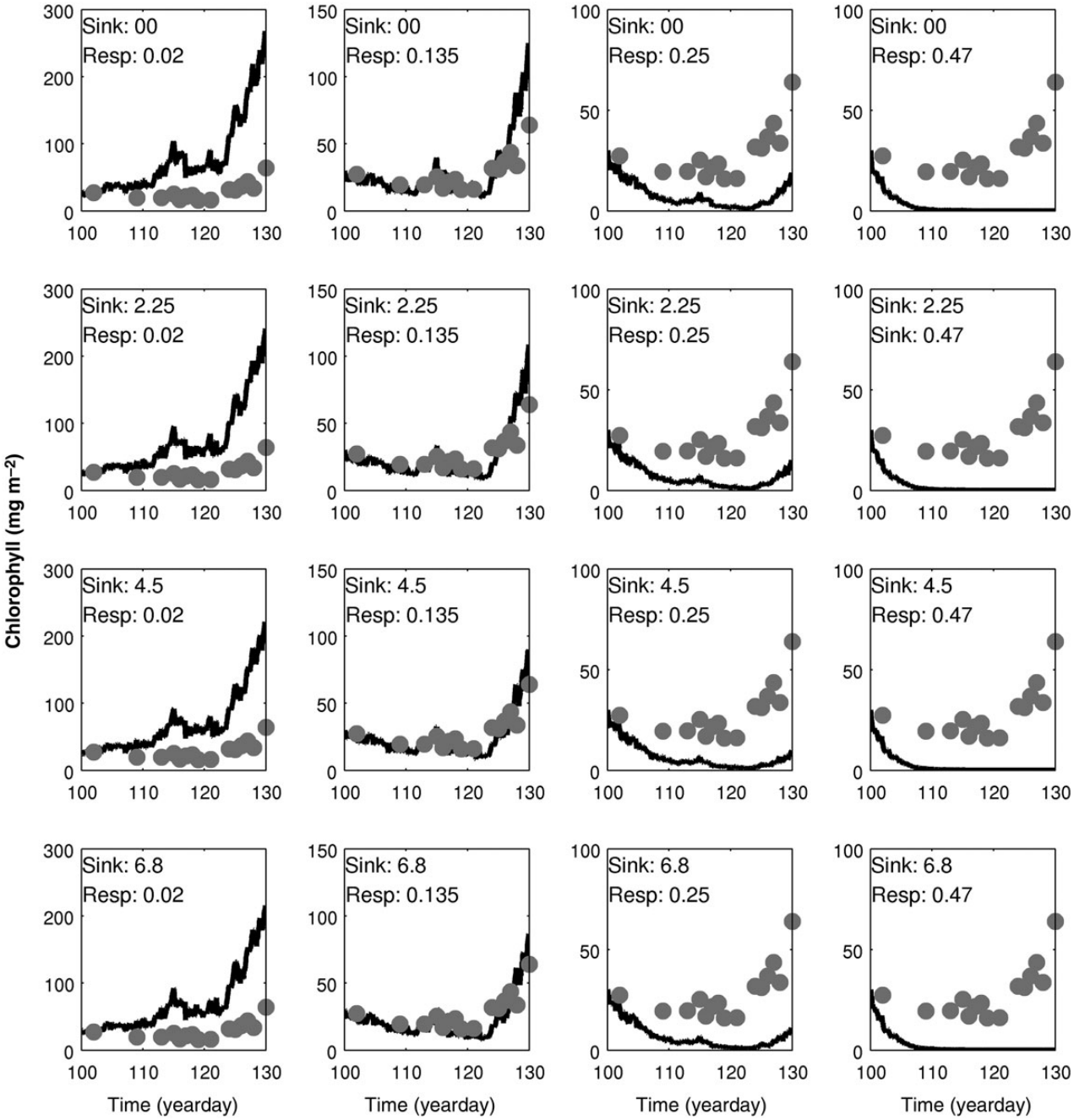

Figure 5. Simulated 100 m integrated chlorophyll at Ocean Weathership Mike using different combinations of fixed values for carbon-specific respiration rate (0.02, 0.135, 0.35, 0.47 d^{-1}) and fixed sinking rates (0.0, 2.25, 4.5, 6.8 m d^{-1}). The grey dots indicated measured values.

velocities can be approximately several hundred meters per day (Marshall and Schott, 1999; D'Asaro, 2008) thus greatly exceeding sinking rates. Nevertheless, sinking can remain an important aspect, since cells may still sink out at the bottom of the mixed, especially during periods of reduced winter deep convection which is of varying depth and temporal duration (Marshall and Schott, 1999). This is captured in our simulation (Figure 1b). Hence, cells can experience periods without convective mixing, causing increased sinking, and increased detrainment of cells at the base of the convective layer. Convective layer deepening, due to stronger winds and cooling, can lead to an entrainment of previous "lost" cells back into the CML depending on the interaction between sinking rate and convective mixing. For example, D'Asaro (2008) found that the maximum sinking velocity for cells to be successfully re-incorporated into the CML to be 7 m d^{-1}. In this study, lower sinking rates (0.13–3.7 m d^{-1}) were recorded near the surface, generally staying below 2 m d^{-1}.

Towards the end of the simulation when environmental conditions became more favourable for growth and stratification had commenced, sinking rates in the upper 50 m ranged between 0.13 and 1.1 m d^{-1} (Figure 3b). Sinking rates below the mixed-layer depth remained relatively constant at the maximum of 6.8 m d^{-1}.

These rates cover a wide range of sinking rates reported for different taxa and environmental conditions (Smayda, 1970) incorporating the assumption of lower sinking rates for growing cells (Waite *et al.*, 1992). Our model was not able to reproduce positive buoyancy as reported for large fast growing diatoms (Moore and Villareal, 1996; Acuña *et al.*, 2010). However, in field samples takes during the simulated period diatoms represented only a minor fraction of the phytoplankton composition (Irigoien *et al.*, 1998). Given our simulated values and observed and predicted convective velocities, it is suggested that phytoplankton sinking rates play only a minor role in the loss terms during periods of deep convection. However, it may be of significance for cells during periods of weakening convection. Here phytoplankton cells can be detained below the convective mixing thus having the potential to be lost from the system and sequestered at depth.

Dark respiration

Dark respiration can be highly variable and is known to change with growth and physiological condition of the cell (Waite *et al.*, 1992; Jochem, 1999). In the classical critical-depth model (Sverdrup, 1953) however, as in most models, it is treated as a constant, potentially leading to significant errors (Smetacek and Passow, 1990).

As growth during winter is normally limited by light due to shorter photoperiod and deeper mixing, dark respiration holds the potential to be an important physiology component, impacting on the onset of the spring bloom as well as the winter stock.

Using variable respiration rates, the model estimated higher values of respiration closer to the surface (Figure 3a), where cells exhibit positive growth rates. This is in agreement with our mechanistic understanding of dark respiration (Falkowski and Owens, 1980; Jochem, 1999) and with the reported ratios of respiration to gross growth (Laws and Bannister, 1980; Geider, 1992; Marra and Barber, 2004).

A reduction of the respiratory losses with depth can allow cells to prolong the availability of energetic reserves and thus survival in the dark. During winter in a deep convective layer, this can be an important survival strategy (McMinn and Martin, 2013), potentially playing an important role in determining the seed population for the spring bloom (Backhaus *et al.*, 1999).

Fixed vs. flexible parameterizations

In this study, we contrasted simulations with variable respiration and sinking rates with those using fixed values to highlight the potential importance of the cells response to environmental conditions. Usually in our simulations, comparisons of fixed respiration and sinking rates over the range of values encompassed by our flexible parameterizations were unable to reproduce the observed concentrations (Figure 5). Applying a specific respiration rate of 0.135 d^{-1} showed a similarly good fit to observations. However, this fixed respiration rate, when expressed as respiration in percentage loss per gross growth (Figure 4) is below the value reported for growing cells (Laws and Bannister, 1980; Geider, 1992; Marra and Barber, 2004). Conversely, the adaptive model was able to simulate a realistic gross growth to respiration ratio (Figure 4). This resulted in higher respiration rates near the surface, which needed to be compensated by lower respiration rates at depth (Figure 3a) to achieve similar biomass to the observations (Figure 2). Thus, to reproduce the observed concentrations, the model required employing fixed parameter values of respiration not substantiated in the literature. This indicates that during the winter and the spring transition period acclimation of physiological rates can be an important process to sustain the phytoplankton community.

Conclusion

In this study, we showed, using a Lagrangian phytoplankton IBM which allowed cells to modify physiological rates, that plasticity of physiological rates can play in important role for the persistence and composition of the North Atlantic phytoplankton community.

When using variable respiration and sinking rates, the model was able to capture the observed phytoplankton concentration during deep convective mixing and the timing and magnitude of the onset of the spring bloom (Figure 2), while simulating realistic physiological rates. In contrast, the model with fixed rates was only able to produce the observations when employing unrealistic parameter values. These results highlight the importance of considering variable parameterization in modelling approaches and suggest that the cells ability to adjust physiological rates to environmental conditions may play an important role in the onset of classical phytoplankton spring bloom. The adaptive model was able to maintain a viable phytoplankton biomass over the convective layer during winter similar to that observed by Backhaus *et al.* (2003), with potentially important implications for the carbon budget. Furthermore, minor phytoplankton surface blooms during winter occurred in the absence of stratification due to a reduction in deep convective mixing. Similar features have been observed in the North Atlantic (Townsend *et al.*, 1992) supporting the hypothesis that active mixing can be more important in controlling growth (Taylor and Ferrari, 2011a) than the hydrostatic conditions employed in the classical critical-depth model (Sverdrup, 1953).

Clearly, the biophysical environment sets the boundaries on phytoplankton dynamics and thus plays a central role in phytoplankton community dynamics. However, an organisms ability to acclimatize to these constraints cannot be neglected, as it allows the organism to find loopholes to escape these controls (Chisholm, 1992). To gain a more realistic understanding of phytoplankton dynamics, the interplay between physical and biological controls needs to be merged with advances in our understanding of the physiologically determined adaptive capacities of phytoplankton cells.

Acknowledgements

The observational phytoplankton data used for the validation was kindly provided by X. Irigoien. Meteorological data from station "Mike" was kindly provided by the Norwegian Meteorological Office (METNO). This publication was partly financially supported by the 7th EU-framework project EURO-BASIN (Contract Nr 264933) and the DTU Aqua PhD School.

References

Acuña, J., López-Alvarez, M., Nogueira, E., and González-Taboada, F. 2010. Diatom flotation at the onset of the spring phytoplankton bloom: an in situ experiment. Marine Ecology Progress Series, 400: 115–125.

Anderson, L., and Sweeney, B. 1977. Diel changes in sedimentation characteristics of Ditylum brightwelli: changes in cellular lipid and effects of respiratory inhibitors and ion-transport modifiers. Limnology and Oceanography, 22: 539–552.

Backhaus, J., Hegseth, E., Wehde, H., Irigoien, X., Hatten, K., and Logemann, K. 2003. Convection and primary production in winter. Marine Ecology Progress Series, 251: 1–14.

Backhaus, J., Wehde, H., Hegseth, E., and Kämpf, J. 1999. Phyto-convection: the role of oceanic convection in primary production. Marine Ecology Progress Series, 189: 77–92.

Behrenfeld, M. J. 2010. Abandoning Sverdrup's critical depth hypothesis on phytoplankton blooms. Ecology, 91: 977–989.

Behrenfeld, M. J., and Boss, E. S. 2014. Resurrecting the ecological underpinnings of ocean plankton blooms. Annual Review of Marine Science, 6: 167–194.

Bienfang, P., Harrison, P., and Quarmby, L. 1982. Sinking rate response to depletion of nitrate, phosphate and silicate in four marine diatoms. Marine Biology, 67: 295–302.

Boyd, C., and Gradmann, D. 2002. Impact of osmolytes on buoyancy of marine phytoplankton. Marine Biology, 141: 605–618.

Brookes, J., and Ganf, G. 2001. Variations in the buoyancy response of Microcystis aeruginosa to nitrogen, phosphorus and light. Journal of Plankton Research, 23: 1399–1411.

Chisholm, S. 1992. Phytoplankton size. *In* Primary Productivity and Biogeochemical Cycles in the Sea Environmental Science Research, 43, pp. 213–237. Ed. by P. G. Falkowski, A. D. Woodhead, and K. Vivirito. Plenum Press, New York.

Cloern, J. E., Grenz, C., and Vidergar-Lucas, L. 1995. An empirical model of the phytoplankton chrlorphyll: carbon ratio-the conversion factor between productivity and growth rate. Limnology and Oceanography, 40: 1313–1321.

Cosper, E. 1982. Influence of light intensity on diel variations in rates of growth, respiration and organic release of a marine diatom: comparison of diurnally constant and fluctuating light. Journal of Plankton Research, 4: 705–724.

D'Asaro, E. 2008. Convection and the seeding of the North Atlantic bloom. Journal of Marine Systems, 69: 233–237.

De Boyer Montégut, C., Madec, G., Fischer, A. S., Lazar, A., and Iudicone, D. 2004. Mixed layer depth over the global ocean: an examination of profile data and a profile-based climatology. Journal of Geophysical Research, 109: C12003.

Eilertsen, H., Sandberg, S., and Tollefsen, H. 1995. Photoperiodic control of diatom spore growth: a theory to explain the onset of phytoplankton blooms. Marine Ecology Progress Series, 116: 303–307.

Evans, G., and Parslow, J. 1985. A model of annual plankton cycles. Biological Oceanography, 3: 327–347.

Falkowski, P., Dubinsky, Z., and Wyman, K. 1985. Growth-irradiance relationships in phytoplankton. Limnology and Oceanography, 30: 311–321.

Falkowski, P., and Owens, T. 1980. Light-shade adaptation two strategies in marine phytoplankton. Plant Physiology, 66: 592–595.

Ferrari, R., Merrifield, S. T., and Taylor, J. R. 2014. Shutdown of convection triggers increase of surface chlorophyll. Journal of Marine Systems, in press.

Geider, R. J., and Osborne, B. A. 1989. Respiration and microalgal growth: a review of the quantitative relationship between dark respiration and growth. New Phytologist, 112: 327–341.

Geider, R. 1992. Respiration: taxation without representation? *In* Primary Productivity and Biogeochemical Cycles in the Sea Environmental Science Research, 43, pp. 333–360. Ed. by P. Falkowski, A. Woodhead, and K. Vivirito. Springer, USA.

Geider, R. J., MacIntyre, H. L., and Kana, T. M. 1997. Dynamic model of phytoplankton growth and acclimation: responses of the balanced growth rate and the chlorophyll a: carbon ratio to light, nutrient-limitation and temperature. Marine Ecology Progress Series, 148: 187–200.

Geider, R. J., MacIntyre, H. L., and Kana, T. M. 1998. A dynamics regulatory model of phytoplanktonic acclimation to light, nutrients, and temperature. Limnology and Ocenaography, 43: 679–694.

Gran, H., and Braarud, T. 1935. A quantitative study of the phytoplankton in the Bay of Fundy and the Gulf of Maine (including observations on hydrography, chemistry and turbidity). Journal of the Biological Board of Canada, 1: 219–467.

Große, F., Lindemann, C., Pätsch, J., and Backhaus, J. O. 2014. The influence of winter convection on primary production: a parameterisation using a hydrostatic three-dimensional biogeochemical model. Journal of Marine Systems, Elsevier BV, in press.

Hellweger, F. L., and Kianirad, E. 2007. Individual-based modeling of phytoplankton: evaluating approaches for applying the cell quota model. Journal of Theoretical Biology, 249: 554–565.

Houde, E. D. 2008. Emerging from Hjort's Shadow. Journal of Northwest Atlantic Fishery Science, 41: 53–70.

Huisman, J., van Oostveen, P., and Weissing, F. 1999. Critical depth and critical turbulence: two different mechanisms for the development of phytoplankton blooms. Limnology and Oceanography, 44: 1781–1787.

Irigoien, X., Head, R., Klenke, U., Meyer-Harms, B., Harbour, D., Niehoff, B., Hirche, H., *et al.* 1998. A high frequency time series at weathership M, Norwegian Sea, during the 1997 spring bloom: feeding of adult female Calanus finmarchicus. Marine Ecology Progress Series, 172: 127–137.

Jochem, F. 1999. Dark survival strategies in marine phytoplankton assessed by cytometric measurement of metabolic activity with fluorescein diacetate. Marine Biology, 135: 721–728.

Kämpf, J., and Backhaus, J. O. 1998. Shallow, brine-driven free convection in polar oceans: Nonhydrostatic numerical process studies. Journal of Geophysical Research, 103: 5577.

Kochergin, V. P. 1987. Three dimensional prognostic models. Coastal and Estuarine Sciences, 4: 201–208.

Landry, M. R., and Hassett, R. P. 1982. Estimating the grazing impact of marine micro-zooplankton. Marine Biology, 67: 283–288.

Langdon, C. 1988. On the causes of interspecific differences in the growth-irradiance relationship for phytoplankton. II. A general review. Journal of Plankton Research, 10: 1291–1312.

Laws, E. A., and Bannister, T. T. 1980. Nutrient- and light-limited growth of Thalassiosira fluviatilis in continuous culture, with implications for phytoplankton growth in the ocean. Limnology and Oceanography, 25: 457–473.

Lindemann, C., and St John, M. A. 2014. A seasonal diary of phytoplankton in the North Atlantic. Frontiers in Marine Science, 1: 00037.

Mahadevan, A., D'Asaro, E., Lee, C., and Perry, M. J. 2012. Eddy-driven stratification initiates North Atlantic spring phytoplankton blooms. Science, 337: 54–58.

Marra, J., and Barber, R. T. 2004. Phytoplankton and heterotrophic respiration in the surface layer of the ocean. Geophysical Research Letters, 31: 1–4.

Marshall, J., and Schott, F. 1999. Open ocean convection: observations, theory, and models. Reviews of Geophysics, 37: 1–64.

McDougall, T., Jackett, D., Wright, D., and Feistel, R. 2003. Accurate and computationally efficient algorithms for potential temperature and density of seawater. Journal of Atmospheric and Oceanic Technology, 20: 730–741.

McMinn, A., and Martin, A. 2013. Dark survival in a warming world. Proceedings of the Royal Society B: Biological Sciences, 280: 20122909.

Miklasz, K., and Denny, M. 2010. Diatom sinking speeds: improved predictions and insight from a modified Stokes' law. Limnology and Oceanography, 55: 2513–2525.

Moore, J. K., and Villareal, T. A. 1996. Size-ascent rate relationships in positively buoyant marine diatoms. Limnology and Oceanography, 41: 1514–1520.

Niehoff, B., Klenke, U., Hirche, H., Irigoien, X., Head, R., and Harris, R. 1999. A high frequency time series at weathership M, Norwegian Sea, during the 1997 spring bloom?: the reproductive biology of Calanus finmarchicus. Marine Ecology Progress Series, 176: 81–92.

Peperzak, L., and Colijn, F. 2003. Phytoplankton sinking rates in the Rhine region of freshwater influence. Journal of Plankton Research, 25: 365–383.

Riley, G. A. 1946. Factors controlling phytoplankton populations on Georges Bank. Journal of Marine Research, 6: 54–73.

Sakshaug, E., Andresen, K., and Kiefer, D. 1989. A steady state description of growth and light absorption in the marine planktonic diatom Skeletonema costatum. Limnology and Oceanography, 34: 198–205.

Sakshaug, E., Johnsen, G., Andresen, K., and Vernet, M. 1991. Modeling of light-dependent algal photosynthesis and growth: experiments with the Barents Sea diatoms Thalassiosira nordenskioldii and Chaetoceros furcellatus. Deep Sea Research Part A. Oceanographic Research Papers, 38: 415–430.

Sanders, R., Henson, S. A., Koski, M., De La Rocha, C. L., Painter, S. C., Poulton, A. J., Riley, J., *et al.* 2014. The Biological Carbon Pump in the North Atlantic. Progress in Oceanography. Elsevier Ltd.

Smayda, T. 1970. The suspension and sinking of phytoplankton in the sea. Oceanography and Marine Biology: An Annual Review, 8: 353–414.

Smetacek, V., and Passow, U. 1990. Spring bloom initiation and Sverdrup's critical-depth model. Limnology and Oceanography, 35: 228–234.

Sverdrup, H. 1953. On conditions for the vernal blooming of phytoplankton. Journal du Conseil, 18: 287–295.

Taylor, J. R., and Ferrari, R. 2011a. Shutdown of turbulent convection as a new criterion for the onset of spring phytoplankton blooms. Limnology and Oceanography, 56: 2293–2307.

Taylor, J. R., and Ferrari, R. 2011b. Ocean fronts trigger high latitude phytoplankton blooms. Geophysical Research Letters, 38: L23601.

Townsend, D., Keller, M., Sieracki, M., and Ackleson, S. 1992. Spring phytoplankton blooms in the absence of vertical water column stratification. Nature, 360: 59–62.

Townsend, D. W., Cammen, L. M., Holligan, P. M., Campbell, D. E., and Pettigrew, N. R. 1994. Causes and consequences of variability in the timing of spring phytoplankton blooms. Deep Sea Research Part I: Oceanographic Research Papers, 41: 747–765.

UNESCO, I. W. G. 1981. The practical salinity scale1978 and the international equation of state of seawater 1980. UNESCO Technical Report Papers in Marine Science.

Verity, P. 1982. Effects of temperature, irradiance, and daylength on the marine diatom Leptocylindrus danicus Cleve. III. Dark respiration. Journal of Experimental Marine Biology and Ecology, 60: 197–207.

Waite, A. M., and Nodder, S. D. 2001. The effect of in situ iron addition on the sinking rates and export flux of Southern Ocean diatoms. Deep-Sea Research Part II: Topical Studies in Oceanography, 48: 2635–2654.

Waite, A. M., Thompson, P. A., and Harrison, P. J. 1992. Does energy control the sinking rates of marine diatoms? Limnology and Oceanography, 37: 468–477.

Walter, B., Peters, J., van Beusekom, J. E. E., and St John, M. A. 2015. Interactive effects of temperature and light during deep convection: a case study on growth and condition of the diatom Thalassiosira weissflogii. ICES Journal of Marine Science, 72: 2061–2071.

Weger, H., Herzig, R., Falkowski, P., and Turpin, D. 1989. Respiratory losses in the light in a marine diatom: measurements by short-term mass spectrometry. Limnology and Oceanography, 34: 1153–1161.

Wehde, H., and Backhaus, J. 2000. The fate of Lagrangian tracers in oceanic convective conditions: on the influence of oceanic convection in primary production. Nonlinear Analysis: Real World Applications, 1: 3–21.

Wehde, H., Backhaus, J. O., and Nøst Hegseth, E. 2001. The influence of oceanic convection in primary production. Ecological Modelling, 138: 115–126.

Xue, X., Gauthier, D. A., Turpin, D. H., and Weger, H. G. 1996. Interactions between photosynthesis and respiration in the green alga Chlamydomonas reinhardtii (characterization of light-enhanced dark respiration). Plant Physiology, 112: 1005–1014.

Handling editor: Shubha Sathyendranath